Formation of electron kappa distributions due to interactions with parallel propagating whistler waves

X. Tao and Q. Lu

Citation: Physics of Plasmas (1994-present) **21**, 022901 (2014); doi: 10.1063/1.4865574
View online: http://dx.doi.org/10.1063/1.4865574
View Table of Contents: http://scitation.aip.org/content/aip/journal/pop/21/2?ver=pdfcov
Published by the AIP Publishing

Formation of electron kappa distributions due to interactions with parallel propagating whistler waves

X. Tao[1,2,a] and Q. Lu[1,2]
[1]CAS Key Laboratory of Geospace Environment, Department of Geophysics and Planetary Sciences, University of Science and Technology of China, Hefei, Anhui 230026, China
[2]Mengcheng National Geophysical Observatory, School of Earth and Space Sciences, University of Science and Technology of China, Hefei, Anhui 230026, China

(Received 19 November 2013; accepted 31 January 2014; published online 14 February 2014)

In space plasmas, charged particles are frequently observed to possess a high-energy tail, which is often modeled by a kappa-type distribution function. In this work, the formation of the electron kappa distribution in generation of parallel propagating whistler waves is investigated using fully nonlinear particle-in-cell (PIC) simulations. A previous research concluded that the bi-Maxwellian character of electron distributions is preserved in PIC simulations. We now demonstrate that for interactions between electrons and parallel propagating whistler waves, a non-Maxwellian high-energy tail can be formed, and a kappa distribution can be used to fit the electron distribution in time-asymptotic limit. The κ-parameter is found to decrease with increasing initial temperature anisotropy or decreasing ratio of electron plasma frequency to cyclotron frequency. The results might be helpful to understanding the origin of electron kappa distributions observed in space plasmas. © *2014 AIP Publishing LLC*. [http://dx.doi.org/10.1063/1.4865574]

I. INTRODUCTION

The velocity distribution of charged particles in space plasmas like solar wind and planetary magnetospheres frequently exhibits a non-Maxwellian high-energy tail.[1–5] This population is often modeled by a kappa-type distribution function, a list of which can be found in Ref. 6. A brief summary of observations and related theories about kappa distributions in space plasmas is given in a recent review by Pierrard and Lazar.[7] These kappa distributions might have important implications in wave-particle interaction processes,[8–11] and understanding the origin of the high-energy tail and the kappa distribution is an on-going research topic. Various mechanisms, including those due to inhomogeneity[12] or stochastic acceleration due to plasma turbulence,[13–17] have been proposed to explain the formation of kappa distributions and the related acceleration of charged particles. In this paper, we are mainly concerned with the possibility of forming electron kappa-type distributions due to interactions with plasma waves.

One of the plasma wave modes that can give rise to electron kappa distributions is whistler mode waves. Ma and Summers[14] solved the Fokker-Planck equation to determine the steady-state distribution of electrons and found that for the given initial Kolmogorov-type wave power distribution, the distribution of electrons is found to be a kappa distribution. Vocks *et al.*[15] took a similar non-self-consistent approach and solved Boltzmann-Vlasov kinetic equation for electron distributions due to interactions with whistler waves, and reached at similar conclusions that whistler waves can lead to formation of halo population of electrons in solar wind. However, as pointed out by Yoon *et al.*,[16] one disadvantage of using a non-self-consistent approach is that the solution of the steady-state distribution depends on the choice of the wave power spectrum. Hence, it is important to use a fully self-consistent approach to investigate the formation of κ-type distributions due to interactions with whistler waves without assuming a pre-existing specific wave power spectrum.

The evolution of electron distributions in generation of whistler waves was treated in a self-consistent way by Gary and Wang[18] using particle-in-cell (PIC) simulations. The authors showed that interactions between electrons and parallel propagating whistler waves preserve the bi-Maxwellian character of electron velocity distributions through PIC simulations. No high-energy tail of electrons was reported by Gary and Wang,[18] which is probably due to the focus only on the thermal part of the electron distribution by the authors. On the other hand, Gary *et al.*[19] used 2D PIC simulations and demonstrated that in case of small parallel plasma beta and oblique whistler waves, where Landau resonance becomes important, a high-energy tail in parallel velocity distribution can be clearly developed. The resulting distribution, however, cannot be modeled by a kappa distribution.

The motivation of this study is to revisit the work by Gary and Wang[18] and to investigate, for the case of parallel propagating whistler waves, whether a kappa distribution can be used to better model the electron distribution in time-asymptotic limit. We focus specially on the high-energy tail of electrons formed in this process due to cyclotron resonant interactions between electrons and whistlers. In Sec. II, we briefly discuss our simulation model. A case study of the evolution of electron distributions is presented in detail in Sec. III A. A possible explanation of the difference between our results and those of Ref. 19 is given. The dependences of the κ-parameter on the initial temperature anisotropy and the ratio of the electron plasma frequency to cyclotron frequency

[a]Electronic mail: xtao@ustc.edu.cn

are demonstrated in Sec. III B. Our results are then summarized in Sec. IV.

II. SIMULATION MODEL

We employ a standard one dimensional PIC simulation model, in which the spatial variation is allowed only in z direction but velocities are three dimensional. In this model, particle's phase space coordinates are updated by solving relativistic Lorentz equations using leapfrog-Boris algorithm.[20] Currents are deposited at simulation girds, where Maxwell equations are solved by a finite difference time domain method to obtain electromagnetic fields. In our code, the background magnetic field $\boldsymbol{B}_0$ is in the z direction. Only parallel propagating waves with wave vector $\boldsymbol{k} \parallel \boldsymbol{B}_0$ are allowed. Periodic boundary conditions of particles and fields are employed. Since we are only interested in whistler waves, ions are treated as fixed.

In all simulations below, we use 1024 cells with cell size $\Delta z = 0.05\, c\Omega_e^{-1}$. Because we are mainly interested in the time-asymptotic behavior of electron distributions, we run all simulations for $1000\,\Omega_e^{-1}$ with time step $\Delta t = 0.02\,\Omega_e^{-1}$. Here, c is the speed of light in vacuum and Ω_e is the electron cyclotron frequency. We use 2000 electrons per cell to reduce numerical noise in electron velocity space distributions.

Only a single bi-Maxwellian distribution of electrons with certain temperature anisotropy is used in the simulation. According to, for example, Ref. 21, this distribution will generate a spectrum of whistler waves with a maximum frequency $\omega^*/\Omega_e = A/(A+1)$, where $A \equiv T_\perp/T_\parallel - 1$ is the temperature (T) anisotropy of a bi-Maxwellian distribution. Here, subscripts $\perp$ and $\parallel$ are perpendicular and parallel directions with respect to the background magnetic field, respectively. Since we only allow parallel propagation of waves, the resulting whistler waves are right-hand circularly polarized with $|\delta B_x|/|\delta B_y| = 1$, as shown by Ref. 19. Here, $|\delta B_i|$ denotes the amplitude of δB_i. The evolution of the whistler wave spectrum and the corresponding wave particle interaction process in a 1D PIC simulation have been studied in detail in a previous work.[21]

III. RESULTS

A. A case study

In this section, we present detailed study and analysis of a "nominal" case. The physical parameters of this case are taken from Ref. 18. Since we use relativistic equations of motion for electrons, the temperature anisotropy is $A \equiv (u_\perp/u_\parallel)^2 - 1$, where $u = \gamma v$ with v the velocity and γ the relativistic factor. For parameters used in this case, however, $\gamma \approx 1$. The initial temperature anisotropy $A = 2$ with parallel plasma beta $\beta_\parallel = 8\pi n_e T_\parallel/B_0^2 = 1.0$. Here, n_e is the electron density. The plasma frequency $\omega_{pe} = 8\Omega_e$.

Shown in Figure 1 is the evolution of $T_\perp/T_\parallel$ and different components of averaged magnetic field intensity K_B, which is defined as

$$K_B = \sum_{i=0}^{N_g-1} \delta B_i^2/N_g B_0^2. \tag{1}$$

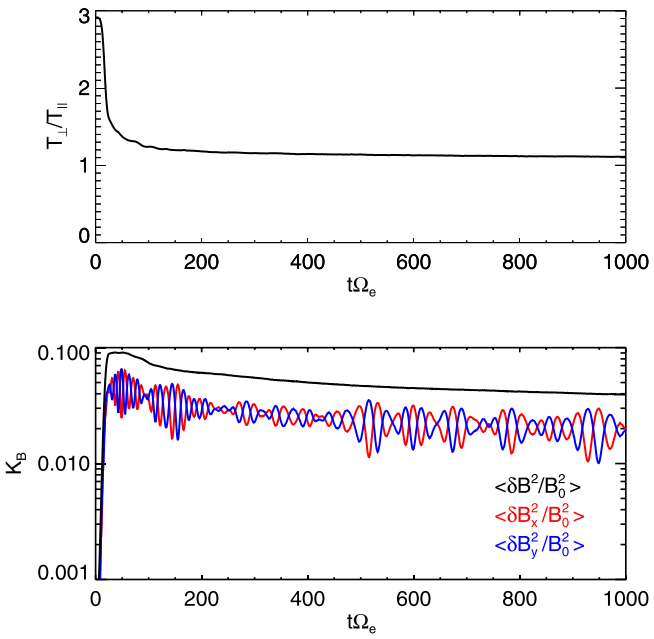

FIG. 1. The evolution of $T_\perp/T_\parallel$ (top) and different components of spatially average normalized magnetic field energy density (bottom) in the nominal case.

Here, the summation is over all grid points and N_g is the total number of grid points. The temperature anisotropy decreases rapidly with time in the growth phase ($t\Omega_e \lesssim 20$), and very slowly after saturation ($t\Omega_e \gtrsim 100$). The relaxation of the temperature anisotropy leads to the decrease in the maximum unstable frequency ω^* and the damping of higher frequency modes in the system. This causes the slow decrease in the wave intensity $\delta B^2 = \delta B_x^2 + \delta B_y^2$ after saturation, as noted by Ossakow *et al.*[21] A similar slow decrease in wave magnetic field energy density has been observed for electromagnetic ion cyclotron waves (EMIC) waves and explained in a similar way by Seough and Yoon.[22] Figure 1 also shows that $|\delta B_x^2| \sim |\delta B_y^2|$, consistent with theories of whistler wave instabilities.[19]

Figure 2 shows reduced distributions of electrons as a function of perpendicular or parallel velocity at three different times ($t\Omega_e = 20$, 400, 1000). The initial distributions of electrons are shown in dashed lines, and distributions from PIC simulations are shown in black sold lines. Blue lines are fittings using a Maxwellian distribution function $g_M(x) = C_M \exp(-x^2/x_T^2)$, and red lines are fittings using a 1D kappa distribution function $g_\kappa(x) = C_\kappa(1 + x^2/\kappa\theta^2)^{-(\kappa+1)}$. Here, $C_M, x_T, C_\kappa, \kappa$, and θ are all fitting parameters. Note that the kappa distribution function becomes a Maxwellian distribution as $\kappa \to \infty$. To compare the goodness of fitting, we calculate the chi-squared parameter defined by

$$\chi^2 = \sum_i (g(i) - g_f(i))^2/g_f(i), \tag{2}$$

where g_f is either g_M or g_κ. In the time-asymptotic limit, as represented by $t\Omega_e = 1000$, Figure 2 shows that for both $g(u_\perp)$ and $g(u_\parallel)$, the kappa distribution function provides better fitting than the Maxwellian distribution function. For $u_\perp$-distribution, the fitting parameter $\kappa_\perp = 18.6$ at $t\Omega_e = 1000$, and

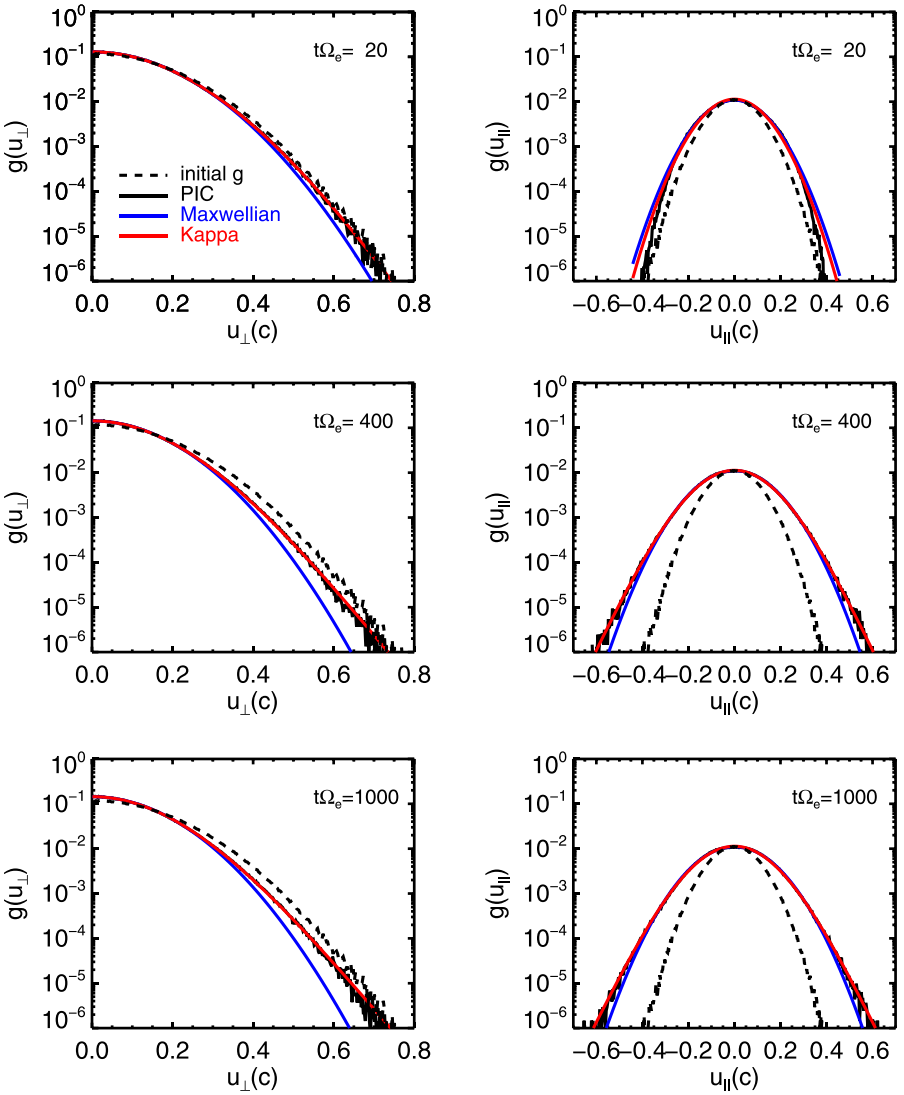

FIG. 2. Snapshots of reduced distributions as a function of perpendicular velocity (left) or parallel velocity (right) at $t\Omega_e = 20$ (top), 400 (middle), and 1000 (bottom). Electron distributions from the PIC simulation are shown in black, together with fittings using a Maxwellian distribution function in blue and a kappa distribution function in red. The initial distribution is shown in dashed lines.

$\chi^2 = 1.72 \times 10^{-2}$ for the Maxwellian distribution, and 1.82×10^{-3} for the kappa distribution. For $u_\parallel$-distribution, the fitting parameter $\kappa_\parallel = 23.9$, and $\chi^2 = 4.78 \times 10^{-3}$ for the Maxwellian distribution, and 9.79×10^{-4} for the kappa distribution. Although the deviation from the Maxwellian distribution is small in this case, the presence of a non-Maxwellian high-energy tail, which can be better fitted by a kappa distribution, is clear. This conclusion is different from that of Ref. 18, probably because Gary and Wang[18] focused on the thermal part of the electron distributions only. The resulting electron distribution from interactions with whistler waves can be better modeled using a kappa distribution function than a Maxwellian distribution, even though we started the simulation with a bi-Maxwellian distribution of electrons.

Figure 2 also demonstrates that in terms of the goodness of modeling by kappa distribution functions, the $u_\parallel$- and $u_\perp$-distributions are different. The $u_\perp$-distribution can be well modeled by a kappa distribution at all three times. The $u_\parallel$-distribution, however, can be well modeled by a kappa distribution only at $t\Omega_e = 400$ and 1000, after the saturation of the wave field (see Figure 1). The $u_\parallel$-distribution cannot be well fitted by either a kappa distribution or a Maxwellian distribution at $t\Omega_e = 20$. The parameter $\chi^2 \approx 0.03$ for $g_\kappa(u_\parallel)$ and 0.04 for $g_M(u_\parallel)$. There is much less important heating for electrons with $u_\parallel \gtrsim 0.3c$ than those with $0.1c \lesssim u_\parallel \lesssim 0.3c$. The acceleration of electrons with $u_\parallel \gtrsim 0.3c$ is only significant in plots for $t\Omega_e = 400$ and 1000. To understand the evolution of the $u_\parallel$-distribution, we plot in Figure 3 the frequency-time power spectral density (PSD) of the wave magnetic field recorded at an arbitrarily chosen point, since the system is

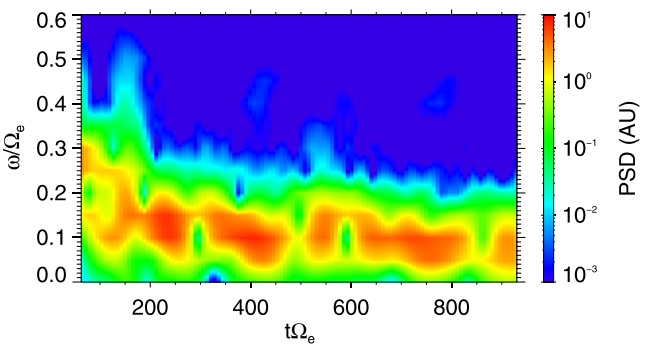

FIG. 3. The frequency-time spectrogram obtained using wave magnetic fields recorded at an arbitrary spatial point. Color-coded is the wave magnetic field PSD in arbitrary units.

homogeneous. Note that the resonant velocity range of $v_\parallel$ is determined by the cyclotron resonance condition

$$\omega - k_\parallel v_\parallel^{\mathrm{R}} = \Omega_e, \tag{3}$$

where ω is the frequency and $k_\parallel$ is the parallel wave number. Using high-density approximation of the cold plasma whistler dispersion relation, the resonant velocity is given by[23]

$$\frac{v_\parallel^{\mathrm{R}}}{c} = \frac{(\Omega_e - \omega)^{3/2}}{\omega_{pe}\omega^{1/2}}. \tag{4}$$

Equations (3) and (4) indicate that for a given spectrum of waves, there is a limit on the range of $v_\parallel^{\mathrm{R}}$ that can be affected by resonant wave-particle interactions. On the other hand, there is no such limit on $v_\perp$ in the non-relativistic case, hence the wave field can resonantly interact with electrons with a broad range of $v_\perp$. This might be one possible reason for the difference in fitting of $u_\perp$- and $u_\parallel$-distributions using a kappa distribution function shown in Figure 2. Note that from Eq. (4), the resonant velocity is inversely proportional to whistler wave frequency ω. Figure 3 shows that at $t\Omega_e = 20$, there is insignificant wave power for $\omega \lesssim 0.1\Omega_e$, while after $t\Omega \gtrsim 50$, there is significant wave power even for $\omega \approx 0.05\Omega_e$. Using simulation parameters of this case, we have for $\omega = 0.1\Omega_e$, $v_\parallel^{\mathrm{R}} = 0.34c$, and for $\omega = 0.05\Omega_e$, $v_\parallel^{\mathrm{R}} = 0.52c$. These numbers are roughly consistent with the range of $u_\parallel$ that shows significant heating at different times in Figure 2.

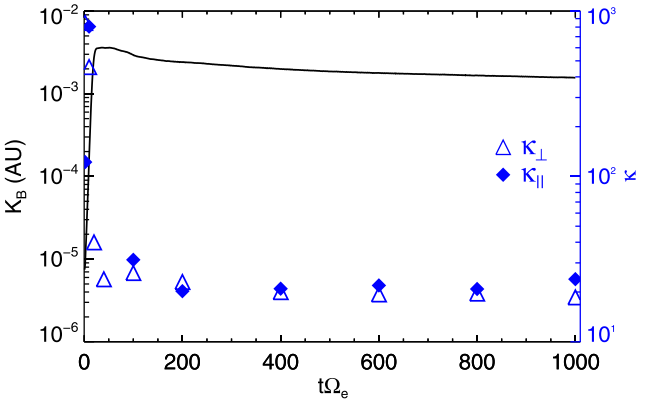

FIG. 4. The evolution of the average wave magnetic field density K_B (black), $\kappa_\perp$ (blue triangle), and $\kappa_\parallel$ (filled blue diamonds) in the nominal case.

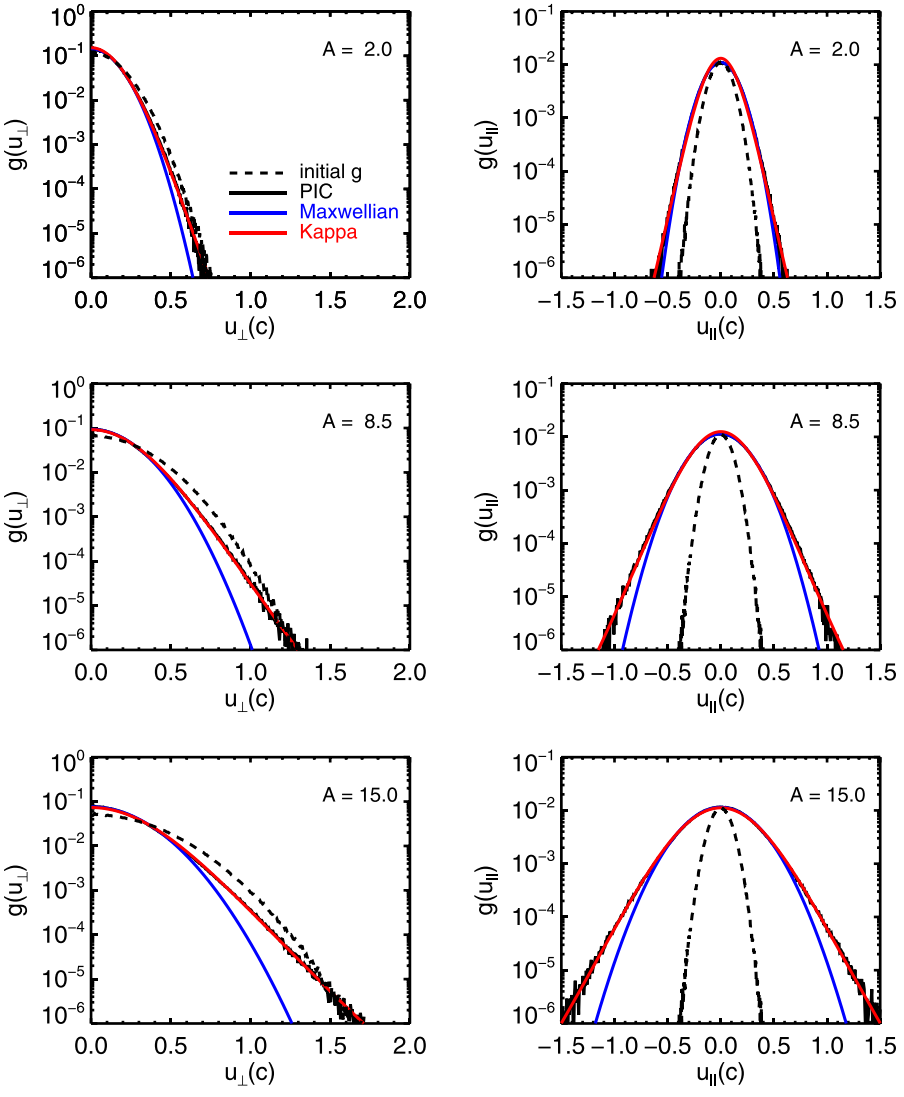

FIG. 5. Snapshots of reduced distributions as a function of perpendicular velocity (left) or parallel velocity (right) for $A = 2.0$ (top), 8.5 (middle), and 15.0 (bottom). Electron distributions from PIC simulations are shown in black, together with fittings using a Maxwellian distribution function in blue and a kappa distribution function in red. The initial distribution is shown in dashed lines.

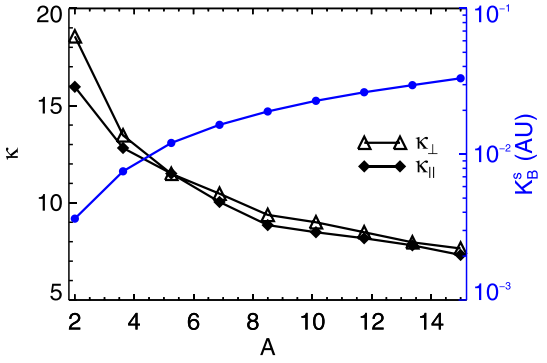

FIG. 6. The dependence of $\kappa_\perp$ (triangle) and $\kappa_\parallel$ (filled diamonds) on the initial temperature anisotropy. Blue line is the saturation wave intensity.

The different dependences of $v_\parallel^R$ on ω in case of cyclotron and Landau resonant interactions might be one possible reason for the different conclusions of this work and those of Ref. 19. Gary *et al.*[19] investigated the evolution of electron distributions interacting with oblique whistler waves where Landau resonance is very important. They found that the resulting $v_\parallel$-distribution of electrons cannot be well modeled by either a kappa distribution or a Maxwellian distribution, because there is no significant heating for electrons with higher parallel velocities. For Landau resonance, the resonance condition is $\omega - k_\parallel v_\parallel^R = 0$. Using quasi-longitudinal approximation of whistler waves and $\omega \ll \Omega_e$, $v_\parallel$ decreases with decreasing ω. Therefore with shifting of wave spectrum toward lower wave frequency, the range of $v_\parallel^R$ that can be affected by Landau resonance also shifts toward smaller parallel velocities. This makes heating of electrons with large $v_\parallel$ by Landau resonance ineffective, and the resulting $v_\parallel$-distribution cannot be well modeled by either a kappa distribution or a Maxwellian distribution.

The evolution of $\kappa_\perp$ and $\kappa_\parallel$ indices is shown in Figure 4, together with average wave magnetic field energy density K_B in arbitrary units. Because the $u_\parallel$-distribution cannot be well fitted by a kappa distribution near the saturation phase, we remove the $\kappa_\parallel$ indices at $t\Omega_e = 20$ and 40. The evolution of K_B is usual showing the initial linear phase and then the saturation stage starting from about $t = 20\Omega_e^{-1}$. At the beginning of the simulation, $\kappa_\perp$ and $\kappa_\parallel$ are close to 1000,

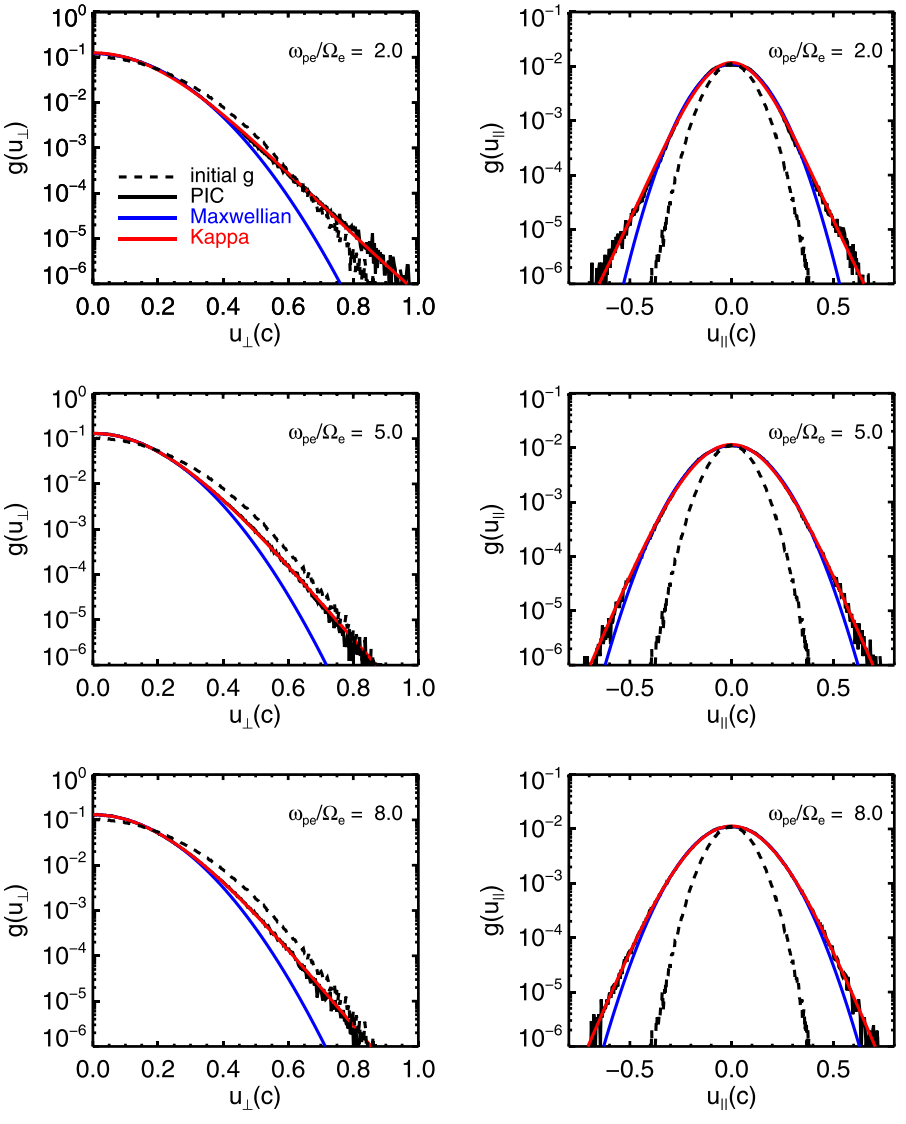

FIG. 7. Snapshots of reduced distributions as a function of perpendicular velocity (left) or parallel velocity (right) for $\omega_{pe}/\Omega_e = 2.0$ (top), 5.0 (middle), and 8.0 (bottom). Electron distributions from PIC simulations are shown in black, together with fittings using a Maxwellian distribution function in blue and a kappa distribution function in red. The initial distribution is shown in dashed lines.

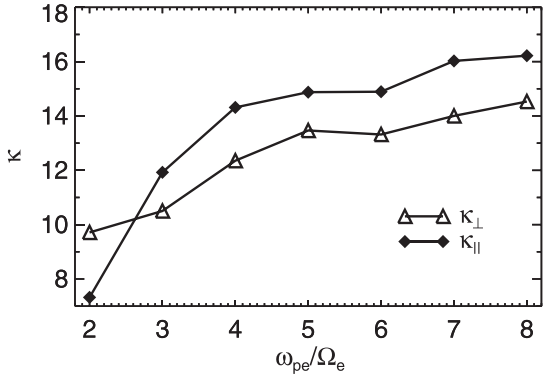

FIG. 8. The dependence of $\kappa_\perp$ (triangle) and $\kappa_\parallel$ (filled diamonds) on the ratio of electron plasma frequency to electron cyclotron frequency ω_{pe}/Ω_e.

consistent with that the distribution is Maxwellian. At $t = 20\Omega^{-1}$, $\kappa_\perp \approx 40$ indicating the formation of the high-energy tail. The indices $\kappa_\perp$ and $\kappa_\parallel$ stay roughly the same after $t\Omega_e = 200$. The time-asymptotic values of $\kappa_\perp$ and $\kappa_\parallel$ are near 20.

B. Dependences of κ index on the initial temperature anisotropy and ω_{pe}/Ω_e

The value of the κ index depends on various plasma parameters. While we cannot scan the full parameter space using PIC simulations, we demonstrate here the dependences of $\kappa_\perp$ and $\kappa_\parallel$ on the initial temperature anisotropy and ω_{pe}/Ω_e. Figure 5 shows $u_\perp$- and $u_\parallel$-distributions of electrons at $t\Omega_e = 1000$ for three runs with different initial temperature anisotropies and $\omega_{pe}/\Omega_e = 8$. In all three cases, the kappa distribution function can better fit the electron distribution function than the Maxwellian distribution function. Also, it is shown that the deviation becomes more significant as A increases. The dependence of $\kappa_\perp$ and $\kappa_\parallel$ on A is shown in Figure 6. The blue dots in Figure 6 are the corresponding saturation wave intensity K_B^s. Figure 6 indicates that a larger initial temperature anisotropy results in larger saturation wave amplitude. Therefore, electrons experience stronger pitch angle and energy scattering in simulations with larger initial temperature anisotropy, leading to a distribution that is more different from a Maxwellian.

Figure 7 shows velocity distributions of electrons at $t\Omega_e = 1000$ for three runs with different ω_{pe}/Ω_e and $A = 3$. The deviation from a Maxwellian distribution becomes more significant as ω_{pe}/Ω_e decreases. The dependence of $\kappa_\perp$ and $\kappa_\parallel$ on ω_{pe}/Ω_e is shown in Figure 8. As ω_{pe}/Ω_e decreases from 8 to 2, the $\kappa_\perp$ index decreases from about 14 to about 10 and $\kappa_\parallel$ decreases from about 16 to about 7, again showing more significant deviation from a Maxwellian distribution as ω_{pe}/Ω_e decreases. The two studies about the dependencies of κ-indices on A and ω_{pe}/Ω_e further demonstrate that the bi-Maxwellian character of electron distributions is not necessarily preserved in interactions between electrons and whistler waves, and the deviation from the Maxwellian distribution could be significant depending on plasma parameters.

IV. CONCLUSIONS

In this work, we demonstrated that the bi-Maxwellian character of electron velocity distributions is not preserved in generation of parallel propagating whistler waves using self-consistent PIC simulations. A high-energy tail of electron distributions can be formed in this process, and a κ-type distribution function can better model the resulting electron distribution than a Maxwellian in the time-asymptotic limit. At least for the simulation parameters used, the bi-Maxwellian distribution is not the equilibrium state of electrons if there is enough temperature anisotropy that can drive whistler waves unstable. Our results might explain at least partially why observed distributions of electrons normally deviate from bi-Maxwellian distributions. We also found that the values of the $\kappa_\perp$ and $\kappa_\parallel$ indices decrease with increasing initial temperature anisotropy or decreasing ω_{pe}/Ω_e. Note that, however, in space plasmas, the kappa index typically has a value between 2 and 6. Hence, whether or not the interaction process between electrons and parallel propagating whistler waves alone is efficient enough to give rise to some of the observed κ-distributions is unknown. Finally, we would like to point out that interactions with whistler waves might not necessarily form kappa distributions, since Gary *et al.*[19] showed clearly that the resulting high-energy tail of electrons could not be fitted by kappa-type distributions when Landau-resonance is dominant. It thus might be important to find the conditions of the formation of electron kappa distributions due to interactions with whistler waves. These are beyond the scope of the present work and will be left as a future study.

ACKNOWLEDGMENTS

This work is supported by USTC Grant No. KY2080000018. The authors would like to thank an anonymous referee for many valuable suggestions.

[1]S. J. Bame, J. R. Asbridge, H. E. Felthauser, E. W. Hones, and I. B. Strong, J. Geophys. Res. **72**, 113, doi:10.1029/JZ072i001p00113 (1967).
[2]V. M. Vasyliunas, J. Geophys. Res. **73**, 2839, doi:10.1029/JA073i009p02839 (1968).
[3]J. T. Gosling, J. R. Asbridge, S. J. Bame, W. C. Feldman, R. D. Zwickl, G. Paschmann, N. Sckopke, and R. J. Hynds, J. Geophys. Res. **86**, 547, doi:10.1029/JA086iA02p00547 (1981).
[4]S. P. Christon, D. G. Mitchell, D. J. Williams, L. A. Frank, C. Y. Huang, and T. E. Eastman, J. Geophys. Res. **93**, 2562, doi:10.1029/JA093iA04p02562 (1988).
[5]F. Xiao, C. Shen, Y. Wang, H. Zheng, and S. Wang, J. Geophys. Res. **113**, A05203, doi:10.1029/2007JA012903 (2008).
[6]D. Summers and R. M. Thorne, Phys. Fluids B **3**, 1835 (1991).
[7]V. Pierrard and M. Lazar, Solar Phys. **267**, 153 (2010).
[8]D. Summers and R. M. Thorne, J. Geophys. Res. **97**, 16827, doi:10.1029/92JA01664 (1992).
[9]F. Xiao, Q. Zhou, H. Zheng, and S. Wang, J. Geophys. Res. **111**, A08208, doi:10.1029/2006JA011612 (2006).
[10]Q. Lu, L. Zhou, and S. Wang, J. Geophys. Res. **115**, A02213, doi:10.1029/2009JA014580 (2010).
[11]M. Hellberg, R. Mace, and T. Cattaert, Space Sci. Rev. **121**, 127 (2005).
[12]J. D. Scudder and S. Olbert, J. Geophys. Res. **84**, 2755, doi:10.1029/JA084iA06p02755 (1979).
[13]A. Hasegawa, K. Mima, and M. Duong-van, Phys. Rev. Lett. **54**, 2608 (1985).
[14]C. Ma and D. Summers, Geophys. Res. Lett. **25**, 4099, doi:10.1029/1998GL900108 (1998).

[15]C. Vocks, C. Salem, R. P. Lin, and G. Mann, Astrophys. J. **627**, 540 (2005).
[16]P. H. Yoon, T. Rhee, and C.-M. Ryu, J. Geophys. Res. **111**, A09106, doi:10.1029/2006JA011681 (2006).
[17]C.-M. Ryu, T. Rhee, T. Umeda, P. H. Yoon, and Y. Omura, Phys. Plasmas **14**, 100701 (2007).
[18]S. P. Gary and J. Wang, J. Geophys. Res. **101**, 10749, doi:10.1029/96JA00323 (1996).
[19]S. P. Gary, K. Liu, and D. Winske, Phys. Plasmas **18**, 082902 (2011).
[20]C. K. Birdsall and A. B. Langdon, *Plasma Physics via Computer Simulation*, 1st ed., Series in Plasma Physics (Taylor & Francis, 2004).
[21]S. L. Ossakow, E. Ott, and I. Haber, Phys. Fluids **15**, 2314 (1972).
[22]J. Seough and P. H. Yoon, J. Geophys. Res. **117**, A08101, doi:10.1029/2012JA017645 (2012).
[23]R. A. Helliwell, J. Geophys. Res. **72**, 4773, doi:10.1029/JZ072i019p04773 (1967).